Polyaniline Doped by the New Class of Dopant, Ionic Salt: Structure and Properties

Show-An Chen* and Liang-Chang Lin

Department of Chemical Engineering, National Tsing Hua University, Hsinchu 30043, Taiwan, China

Received July 21, 1994; Revised Manuscript Received October 14, 1994®

ABSTRACT: Polyaniline (PAn) can be doped through a protonation by protonic acids, in addition to an oxidation doping by Lewis acid as for the other conjugated conducting polymers. This work reports the new class of dopant, ionic salt, such as $LiClO_4$, $LiBF_4$, $LiPF_6$, and $Zn(ClO_4)_2$, for PAn. The ionic salt can be used to dope PAn by mixing an ionic salt with PAn in the common solvent 1-methyl-2-pyrrolidone and then casting the solution into a film. The structure and properties of ionic salt doped–PAn are investigated by UV–visible, IR and XPS spectroscopies, dynamic mechanical analysis, scanning electron microscopy, and conductivity measurement. It is found that the PAn therein is doped via pseudoprotonation of the imine nitrogen by the metal cation. As in the case of HCl-doped PAn, polarons/bipolarons are generated as reflected in the presence of UV–visible absorption peaks at 420 and 865 nm. The $LiBF_4$-doped PAn film retains a conductivity at the level of 10^{-2} S/cm in the temperature range 25–140 °C. The conductivity then decays to 10^{-3} S/cm as temperature increases to 175 °C, resulting from the increased ring distorsion in the PAn subchains due to the glass transition.

Introduction

Polyaniline (PAn) is an important conducting polymer because of its good environmental stability.[1–3] In addition to the oxidation doping as for the other conducting polymers, PAn can also be doped through protonation by exposure to an appropriate protonic acid without changing the number of π–electrons in the polymer, making its properties unique.[1] It can be applied in organic secondary battery and electrochromic display, due to its reversible oxidation/reduction characteristic, and pH sensor, due to its reversible proton-exchange capability.[4] The protonic acid dopants usually used are inorganic acids (such as HCl, H_2SO_4, HBF_4, etc.)[5–7] or organic acids (such as toluenesulfonic acid),[8] while the oxidation dopants are $(NO^+)(PF_6)^-$, $FeCl_3$, H_2O_2, $Sncl_4$, etc.[9]

This work reports the new class of dopant, ionic salt, such as $LiClO_4$, $LiBF_4$, $LiPF_6$ and $Zn(ClO_4)_2$ etc., for PAn (an emeraldine base) and reports the structure and properties of the ionic salt-doped PAn by use of various spectroscopic methods (UV–visible, IR, XPS), conductivity measurements, dynamic mechanical analysis (DMA), and scanning electron microscopy (SEM). The doping is carried out by mixing PAn and ionic salt solutions in 1-methyl-2-pyrrolidone (NMP) and then casting the mixed solution into film. The resulting film with $LiBF_4$ as dopant has a conductivity of 10^{-2} S/cm. The PAn therein is doped via pseudoprotonation of the imine nitrogen by the metal cation without changing the number of π-electrons in the polymer as in the case of HCl-doped PAn.

Experimental Section

1. Chemicals. Aniline, hydrochloric acid, and perchloric acid were synthetic grade from Merck. NMP of synthetic grade was from Ferak Co. Lithium perchlorate, lithium hexafluorophosphate, and ferric chloride were AG grade from Fluka. Lithium tetrafluoroborate and zinc oxide were from Tokyo Chem. Inc. Co. and Merck, respectively. Zinc perchlorate was prepared by adding 6.028 g of zinc oxide slowly into 10 mL of perchloric acid and then adding ~1 L of deionized water moderately until the solution became neutral. After filtration, the water in the filtrate was removed by evaporation followed by drying under dynamic vacuum; powdery zinc perchlorate was thus obtained. The ionic salts $LiClO_4$ and $LiBF_4$, both of anhydrous grade, used for doping were treated by heating at 260 °C (10 °C above the melting point of $LiClO_4$) for 6 h and 100 °C for 12 h under dynamic vacuum, respectively.

The polyaniline hydrochloride powder was synthesized by an oxidative polymerization of aniline in 1 M aqueous HCl with $(NH_4)_2S_2O_8$ as oxidant as described by S.-A.C in previous work,[12] which is similar to the method used by MacDiarmid et al.[13] The powder was converted to PAn (an emeraldine base) by treatment with 1 M aqueous NH_4OH followed by drying under dynamic vacuum.

The ionic salt-doped PAn films were prepared by incorporation of various mole ratios of salt to PAn solution in NMP (1% by weight) to give a clear solution, followed by casting the solution on a Petri dish and drying under dynamic vacuum at 50–60 °C. The ionic salts used were $LiClO_4$, $LiBF_4$, $LiPF_6$, and $Zn(ClO_4)_2$. The oxidant ($FeCl_3$)-doped PAn film was also prepared by the same procedure. The compositions of the resulting films are designated as $[PAn]_x$ salt, where x is the mole ratio of the approximate repeat unit of PAn to salt.

2. Characterization. An ultraviolet–visible–near-infrared spectrophotometer (UV–vis–near-IR; Perkin-Elmer Lambda 19) was used to measure optical absorbances in the wavelength range 250–2000 nm of solid films coated on glass plates or of solutions coated on quartz plates. The spectrophotometer was equipped with a variable-temperature cell to allow for measurement of spectra under vacuum from 25 to 200 °C; the soaking time was 20 min at each specific temperature, and the heating rate was about 1–2 °C/min during heating.

An infrared spectrophotometer (IR; Perkin-Elmer Model 983) was used to identify the chemical structures of PAn, ionic salt-doped PAn, and $FeCl_3$-doped PAn. These samples were examined by coating their thin liquid films on KBr crystal surfaces and then drying under dynamic vacuum at 50–60 °C.

An X-ray photoelectron spectroscope (XPS; Perkin-Elmer Model 1905) with a Mg Kα X-ray source (1253.6 eV photons) was used to measure Li(1s) and N(1s) core-level spectra of $LiBF_4$ powder and $[PAn]_{4.8}LiBF_4$ film. The pressure in the sample chamber was maintained at 10^{-8} bar or lower during measurements. For Li, the binding energies were referenced to a gold target, Au($4f_{7/2}$) = 83.8 eV. The binding energies of N(1s) were referenced to the C(1s) peak at 284.6 eV to compensate for surface charging effect, and the full widths at

* Author to whom correspondence should be addressed.

® Abstract published in *Advance ACS Abstracts,* January 15, 1995.

0024-9297/95/2228-1239$09.00/0

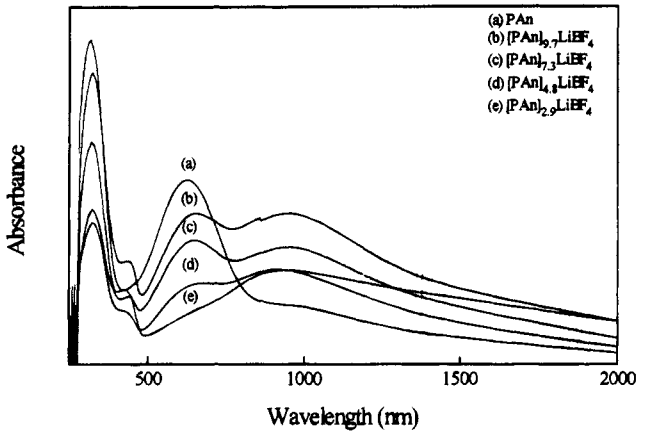

Figure 1. UV–vis absorption spectra of PAn films.

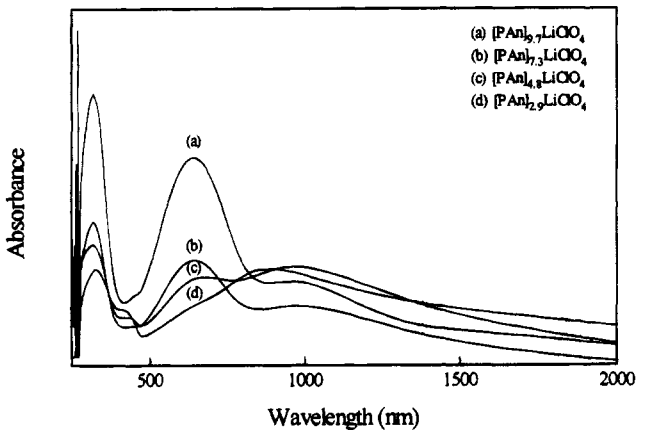

Figure 2. UV–vis absorption spectra of PAn films.

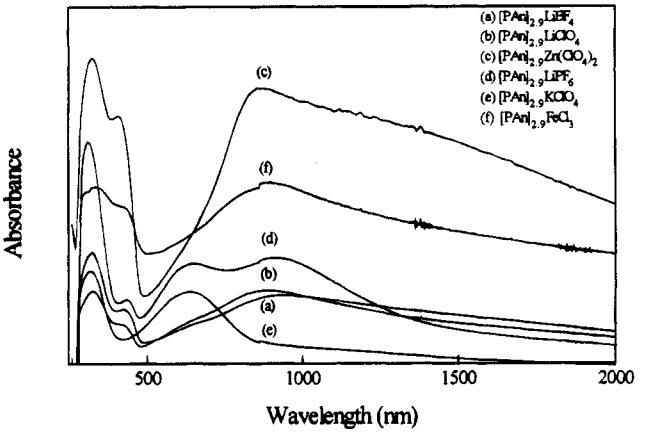

Figure 3. UV–vis absorption spectra of PAn films.

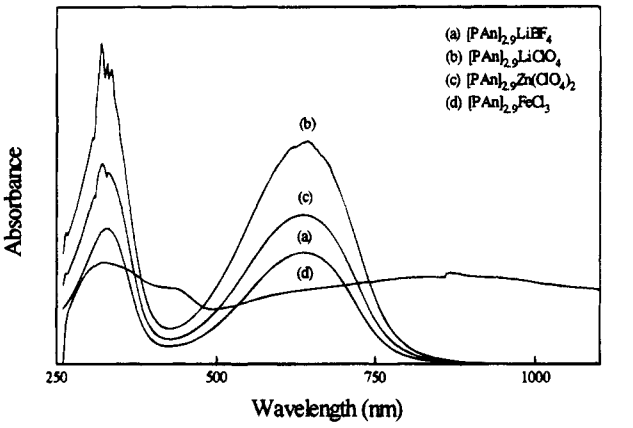

Figure 4. UV–vis absorption spectra of PAn films in NMP solutions (containing 1 wt % PAn).

half-maximum (fwhm) of the Gaussian peak components were kept constant for spectrum deconvolution.

The four-point method[14] was used to measure the conductivity under dry nitrogen atmosphere from 25 to 200 °C with a heating rate of 2 °C/min. Dimensions of the films used were about 10 mm × 10 mm × 0.12 mm. All of the measurements were carried out under dry nitrogen atmosphere.

A dynamic mechanical analyzer (DMA; Du Pont Model 983) was used to measure flexural and loss moduli (E' and E'') of films of PAn and $LiBF_4$-doped PAn in the temperature range −120 to 250 °C with a heating rate of 2 °C/min and frequency 1 Hz. The specimens were about 25 mm long, 10 mm wide, and 0.25 mm thick. After mounting a specimen in the sample chamber, the specimen length subject to cyclic flexural motion was ~2.5 mm.

A scanning electron microscope (SEM; Hitachi Model S-2300) was used to examine morphologies of films of PAn and salt-doped PAn. A piece of film of the about 1 mm × 2 mm in size was fixed on the sample holder using adhesive tape and was then coated with a thin layer of gold to improve image resolution.

Results and Discussion

Ultraviolet–Visible–Near-Infrared (UV–vis–near-IR) Spectroscopy. The UV–vis spectra of films of PAn, $LiBF_4$ doped-PAn, and $LiClO_4$ doped-PAn with the mole ratios of salts to the approximate repeat unit of PAn ($-C_6H_4NH^-$), 1/9.7, 1/7.3, 1/4.8, and 1/2.9, are shown in Figures 1 and 2. The UV–vis spectrum of the PAn has two absorption peaks at 325 and 625 nm, which are due to $\pi-\pi^*$ transition of the benzenoid rings and exciton absorption of the quinoid rings, respectively.[15,16] When N atoms in imine groups are protonated, N and its neighboring quinoid ring become a semiquinoid radical cation,[17] causing a decrease in the exciton absorption peak intensity and a generation of the absorption peaks at about 420 and 865 nm due to the presence of polaron/bipolaron.[17] From Figures 1 and 2, it can be observed that the PAn is doped by the ionic salt as reflected in the generation of the absorption peaks due to polaron/bipolaron at about 420 and 865 nm as in the case of HCl-doped PAn.[17] The intensities of these two peaks and the exciton absorption peak at 625 nm relative to that of the $\pi-\pi^*$ transition at 320 nm also increase and decrease respectively, with increasing salt content.

The other ionic salts, $LiPF_6$ and $Zn(ClO_4)_2$, can also dope PAn, but $KClO_4$ cannot, as can be observed from the UV–vis spectrum in Figure 3 (curve e). If the ionic salt is replaced by the same amount (by mole) of oxidation dopant ($FeCl_3$), the doped PAn film also has UV–vis spectrum (Figure 3, curve f) similar to the ionic-salt-doped PAn but is at the higher doping level. However, doping of PAn by the ionic salt behaves differently from that by the oxidation dopant. For the case with ionic salt, the NMP solution of PAn (1 wt %) with ionic salt is clear and deep-blue in color and has a UV–vis spectrum the same as that without the ionic salt (Figure 4, curves a–c), indicating that no doping occurs. This is due to the solvation of ionic salt by the excess NMP, which can prevent the salt from doping the PAn. When the amount of NMP in the solution decreases during casting, the degree of doping increases. This doping behavior is identical to that in the case of polyacrylic acid/PAn solution in NMP as reported by S.A.C. in previous work.[12,18] For the case with $FeCl_3$, the solution is deep green-blue in color and its UV–vis spectrum (Figure 4, curve d) shows the presence of

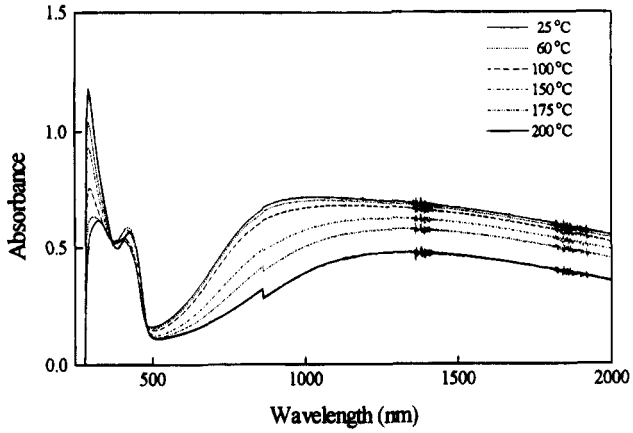

Figure 5. UV–vis absorption spectra of $[PAn]_{2.9}LiClO_4$ at various temperatures from 25 to 200 °C.

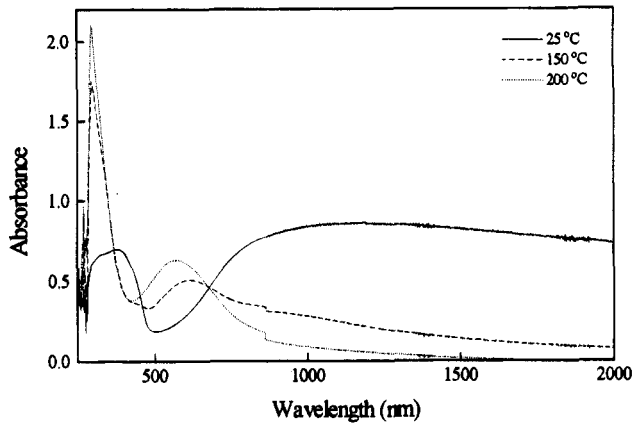

Figure 6. UV–vis absorption spectra of HCl-doped PAn at various temperatures from 25 to 200 °C.

polaron/bipolaron absorptions, indicating an occurrence of doping. On standing for a few seconds, a gellike precipitation is observed in the solution.

In order to investigate whether the minor amount of water in PAn solution could affect the doping behavior, a glass plate coated with a thin solid film of PAn (~0.5 μm) was immersed in a $LiClO_4$-saturated aqueous solution (pH 8.2) for 12 h and then the remnant water was removed by dynamic vacuum pumping. The UV–vis spectra before and after the immersion are nearly the same. This would imply that the protons generated by the hydrolysis of $LiClO_4$ are not enough to provide appreciable doping of PAn. Thus, a minor amount of water in the PAn solution in NMP would have no contribution to the doping.

The UV–vis–near-IR spectra of $[PAn]_{2.9}LiClO_4$ and HCl-doped PAn films with a thickness of ~0.3 ± 0.1 μm in the range 25–200 °C under vacuum are shown in Figures 5 and 6, respectively. For the HCl-doped PAn (Figure 6), when heated from 25 to 150–200 °C, the excitation absorption peak at 625 nm increases and the absorption in the range 700–2000 nm decreases and that of the $\pi-\pi^*$ transition at 320 nm increases, which is due to the thermal undoping through an evolution of the dopant HCl. The HCl-doped PAn film almost converts to the undoped form when heated to 200 °C. However, for the $LiClO_4$-doped PAn (Figure 5), when heated to 200 °C, the absorption in the range 700–2000 nm decreases gradually with temperature; no absorption due to quinoid rings appears during the heating, indicating that the deprotonation-like reaction does not occur. Note that the absorption due to the $\pi-\pi^*$ transition increases with temperature and that due to polaron at ~420 nm is still present at all temperatures. This would indicate an occurrence of a cross-linking reaction through a conversion of the generated quinoid rings (resulting from thermal undoping) to benzenoid rings during the heating.[12] This observation would imply that the ionic salt-doped PAn has better thermal stability due to the nonvolatility of the ionic salts.

Table 1. Characteristic Peaks (cm^{-1}) of the IR Spectra of Doped Polyanilines[a]

sample	stretching mode N=Q=N	N–B–N	C–N	mode of Q=NH^+–B or B–NH^+–B
PAn	1592	1497	1304	1167
$[PAn]_{7.3}LiBF_4$	1590	1498	1306	1165
$[PAn]_{4.8}LiBF_4$	1584	1498	1305	1148
$[PAn]_{2.9}LiBF_4$	1580	1498	1303	1144
$[PAn]_{7.3}LiClO_4$	1588	1496	1305	1148
$[PAn]_{4.8}LiClO_4$	1586	1498	1305	1148
$[PAn]_{2.9}LiClO_4$	1585	1498	1305	1144
$[PAn]_{2.9}Zn(ClO_4)_2$	1580	1497	1303	1146
$[PAn]_{2.9}FeCl_3$	1590	1490	1302	1141

[a] Abbreviations: Q, quinoid unit; B, benzenoid unit.

Infrared Spectroscopy (IR). The main characteristic IR absorptions of PAn, $FeCl_3$-doped PAn, and ionic salt-doped PAn films (which are plasticized with ~15 wt % NMP) are as follows: for NMP, 1700 (C=O stretching) and 1298 cm^{-1} (C–N stretching); for the PAn, 1589 (C=C stretching of quinoid rings),[12] 1496 (C=C stretching of benzenoid rings),[12] 1306 (C–N stretching) and 1165 cm^{-1}, (electronic-like absorption of N=Q=N,[19] where Q denotes the quinoid ring), broad absorption in 2000–4000 (free carriers absorption)[20] and 1145 cm^{-1} (the electronic-like absorption)[19] both due to the doping of PAn. The IR absorption peaks of these films are listed in Table 1. For the $FeCl_3$-doped PAn, the absorption peak of the benzenoid ring stretching shifts by 7 cm^{-1} from 1497 to 1490 cm^{-1}; while that of quinoid ring stretching is almost unchanged. This indicates the occurrence of oxidative doping at the amine nitrogens. For the ionic salt-doped PAn, the quinoid ring stretching shifts by 7–12 cm^{-1} toward lower wavenumbers, and the shifting increases with increasing concentration of ionic salt; while the benzenoid ring stretching is almost unchanged. This indicates that doping by the ionic salt mainly affects the electronic structure of the quinoid units and has no significant effect on the benzenoid units. From the reduction potential table,[21] it is known that Li^+ and Zn^{2+} have rather lower reduction potentials ($V_{red,Li^+} = -3.045$ V, $V_{red,Zn^{2+}} = -0.763$ V) than that of Fe^{3+} ($Fe^{3+} + e^- \rightarrow Fe^{2+}$, $V_{red} = 0.771$ V). Therefore, Li^+ and Zn^{2+} are quite difficult to reduce, with the result that the corresponding oxidation reaction of PAn is not spontaneous. From these observations, we conclude that the ionic salt doping of PAn is not an oxidative doping in nature but is similar to a protonation by protonic acids. Since no protons appear in these systems, the doping must occur because of the pseudoprotonation[22] of the nitrogens in the imine unit by the metal cations. Thus, we propose Scheme 1 for ionic salt doping of PAn. In comparison with the proton-doped PAn, the symmetry-breaking effect of the pseudoprotonation of the metal cation makes it more difficult for electron delocalization to affect the C=C stretching in the benzenoid rings. As a result, its benzenoid ring stretching is almost the same as that of the undoped PAn (Table 1).

X-ray Photoelectron Spectroscopy (XPS). Figure 7 shows the Li(1s) XPS core-level spectra of the ionic

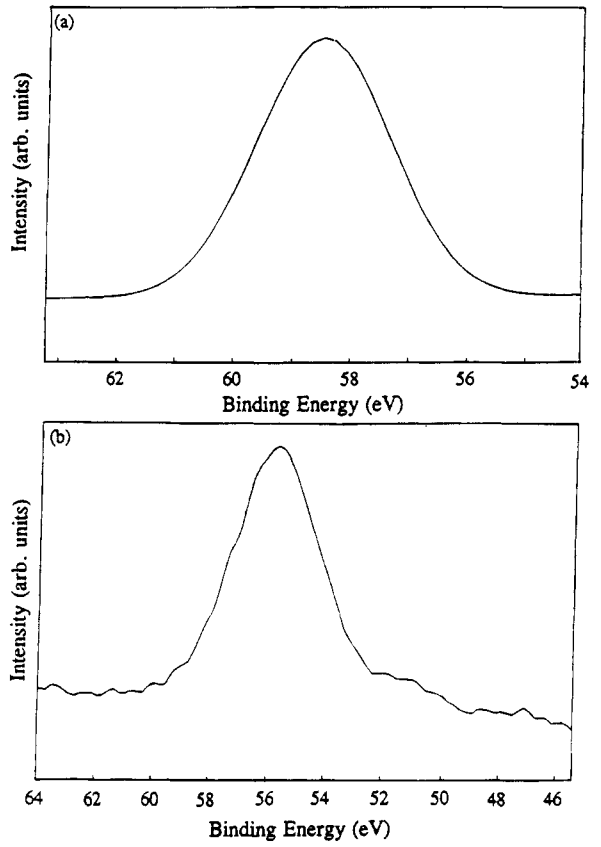

Figure 7. Li(1s) XPS core level spectra of (a) $LiBF_4$ powder and (b) $[PAn]_{4.8}LiBF_4$ film.

Scheme 1

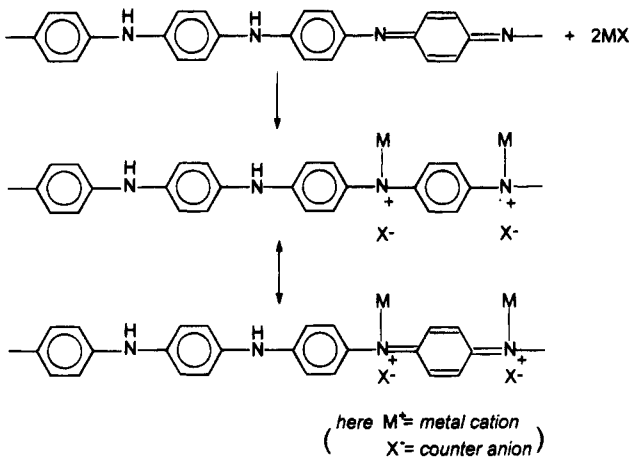

salt, $LiBF_4$ powder, and $[PAn]_{4.8}LiBF_4$ film with the binding energies centered at 58.5 and 56 eV, respectively. In the $[PAn]_{4.8}LiBF_4$ film, no salting out or residual $LiBF_4$ is observed (as noted in the section on SEM). Thus, the salt would not affect the XPS spectra. The binding energy of the Li of $[PAn]_{4.8}LiBF_4$ film is lower by 2.5 eV in comparison with that of $LiBF_4$ powder and is higher by 1 eV in comparison with that of atomic lithium.[23] In other words, in the doped PAn, Li^+ acquires electrons from the PAn molecule chain, resulting in an increase in electron density of the valence level of lithium and therefore in a decrease in binding energy. These observations are in support of the structure of the doped PAn proposed in Scheme 1, in which lithium bonds covalently onto the nitrogens of imine units.

Figure 8 shows the N(1s) XPS core-level spectrum of the $[PAn]_{4.8}LiBF_4$. The spectrum can be deconvoluted into three component peaks centered at 398.2 ± 0.1, 399.3 ± 0.1, and 401 eV; the former two and the latter have fwhm of 1.60 and 1.65 eV, respectively. The area fractions of these peaks are summarized in Table 2.

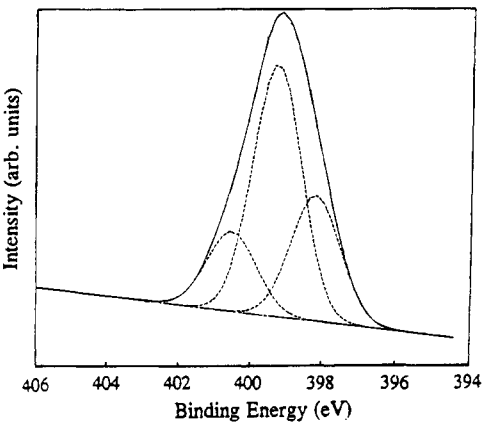

Figure 8. N(1s) XPS core level spectrum of $[PAn]_{4.8}LiBF_4$ film and its deconvolution.

Table 2. N(1s) XPS Results of $[PAn]_{4.8}LiBF_4$ Film

	N(1s) core-level spectrum		
	=N	NH	$NLi^{\bullet+}$
binding energy, eV	398.2 ± 0.1	399.3 ± 0.1	401 ± 0.1
area fraction	0.28	0.55	0.17

Kang et al.[24,25] have pointed out that the N(1s) spectrum of neutral PAn can be deconvoluted into two peaks with same area centered at 398.2 ± 0.1 and 399.3 ± 0.1 eV, which represent the nitrogens of imine and amine units, respectively. When PAn is protonated by HCl, the N(1s) peak generates a tail above binding energy of 401 eV and its imine component at 398.2 eV has decreased area. Kumar and Inoue et al.[26-28] have found that the higher binding energy (BE) can be attributed to the polaron (BE = 400.8 eV) and bipolaron (BE = 402.2 eV). Furthermore, Nakajima et al.[29] have claimed that the tail can be referred to the radical cation ($NH^{\bullet+}$, BE = 400.8 eV) and cationic nitrogen (NH_2^+, BE = 402.3 eV). Thus, for the present ionic salt-doped PAn, the N(1s) peaks at 398.2 and 399.3 eV can be assigned to the imine nitrogen and amine nitrogen, respectively, and that at 401 eV to the generated $NLi^{\bullet+}$ unit, resulting from the pseudoprotonation of the nitrogens of imine units by the Li cations. The doping level of $[PAn]_{4.8}LiBF_4$ film is ~0.17 according to the area fraction of $[NLi^{\bullet+}]$, which is close to the calculated doping level, 0.21. It implies that most of the ionic salt in $[PAn]_{4.8}LiBF_4$ film participate in the doping reaction.

Scanning Electron Micrography (SEM). SEM micrographs of the PAn, $[PAn]_{9.7}LiBF_4$, $[PAn]_{4.8}LiBF_4$, and $[PAn]_{2.9}LiBF_4$ are shown in Figure 9. For the PAn film, the film surface is rather smooth and featureless (Figure 9a); however, after the doping with $LiBF_4$, the films surface show a rough morphology (Figure 9b,c). This rough morphology results from an aggregation of the more rigid doped-PAn subchains. As the $LiBF_4$ content increases to 1/2.9, the excess salt is salted out (Figure 9d). However, at this $LiBF_4$ content, the doping level is still higher than that at 1/4.8 as can be observed from the UV–vis (Figures 1 and 2) and IR results (Table 1). This indicates that the doping at 1/4.8 is still not saturated; thus the film at this doping level is suitable for XPS analysis.

Dynamic Mechanical Analysis (DMA). $[PAn]_x$-$LiBF_4$ films, which were prepared by casting the solution of PAn and $LiBF_4$ in NMP, usually contain residual

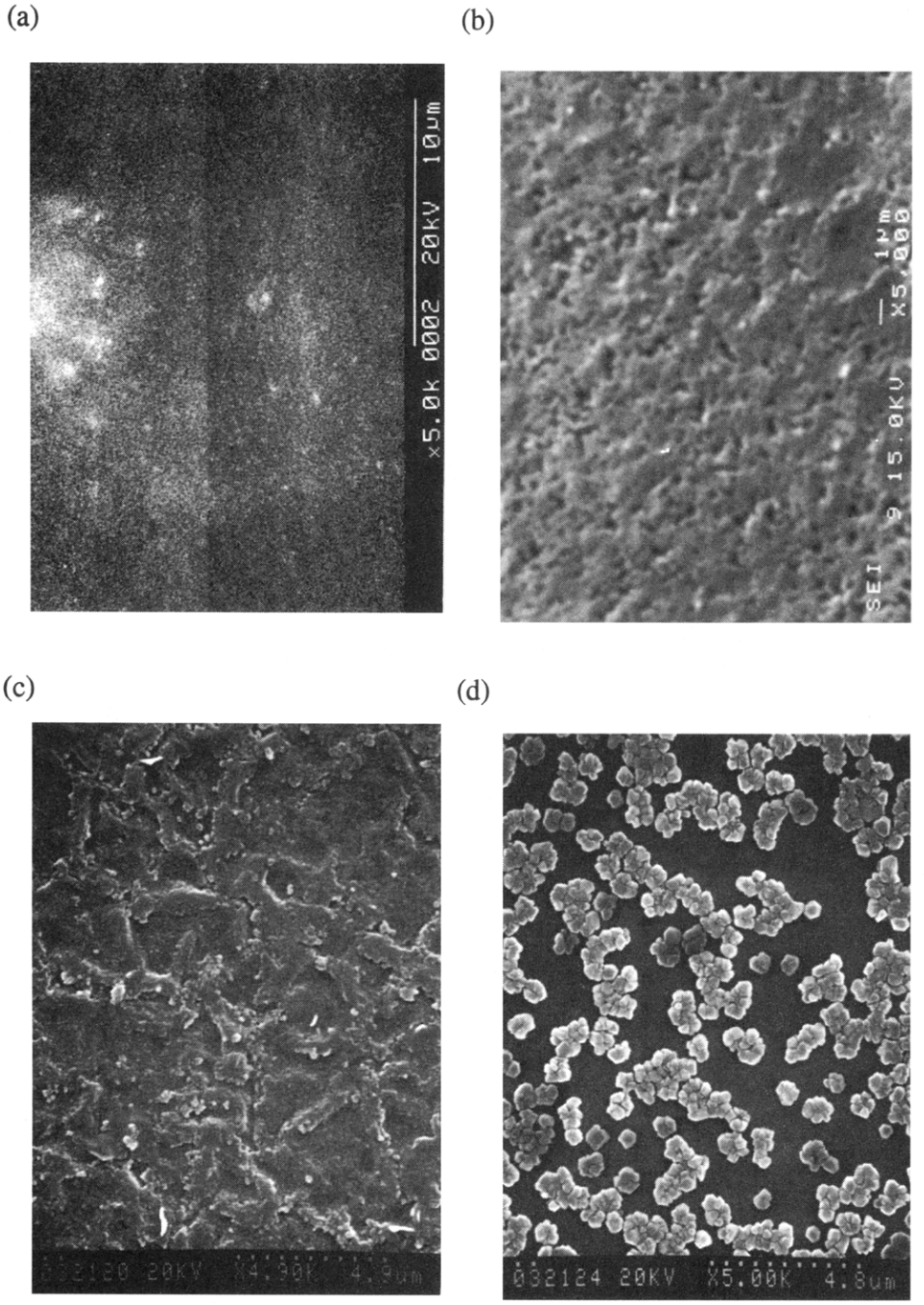

Figure 9. SEM micrographs of (a) PAn, (b) $[PAn]_{9.7}LiBF_4$, (c) $[PAN]_{4.8}LiBF_4$, and (d) $[PAN]_{2.9}LiBF_4$ films.

NMP because of its high boiling point (202 °C) and strong interaction with PAn via hydrogen bonding of the C=O group in NMP with the NH group in PAn as revealed in the previous work by S.-A.C.[12] The NMP contents in the present films with various salt contents and in the PAn film cast from its solution in NMP were determined by a heat scan to 250 °C using a thermagravimetric analyzer (TGA) and are found to be about the same at 12 wt%. DMA results (flexural modulus E' and loss modulus E'') of PAn and ionic salt-doped PAn films are shown in Figure 10. From E'' curves, the two main transitions α and α′ are observed and their characteristic temperatures are listed in Table 3. The transition temperature T_α (97 to 117 °C) determined from E'' can be assigned as the glass transition temperature, because E' drops by 1–2 orders in this transition region. T_α of the PAn and $[PAn]_xLiBF_4$ films with the mole ratios of $LiBF_4$ to the approximate repeat unit of PAn, 1/4.8 and 1/2.9, are 97, 109, 117 °C, respectively (Table 3). The T_α of the doped PAn film increases with the ionic salt content (or doping level) and is higher than that of the neutral PAn film by 12–20 °C. The increase of T_α is due to the more rigid PAn subchains after the doping and the Coulombic interaction between the radical cations on the polymer chains and the N atoms of the PAn chains. As temperature increase beyond the transition region, E' changes from a rapid decrease to a rapid increase until a maximum is reached and then rapid decrease again, where E'' also exhibits similar changes and generates a new peak after the α-transition, which is designated as α′-transition. This α′-transition results from a competition between two factors: (a) increase in stiffness due to further evaporation of NMP and occurrence of cross-linking reaction and (b) decrease in stiffness due to increased segmental thermal motion caused by raising tempera-

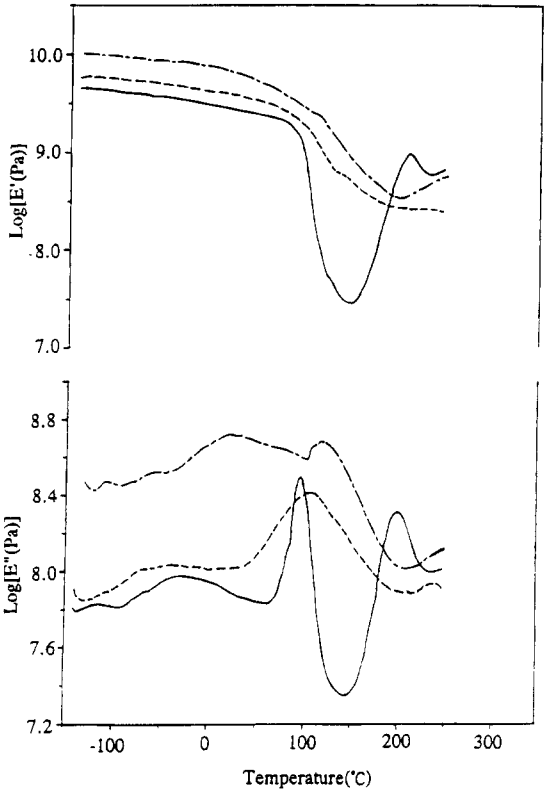

Figure 10. Dynamic mechanical analysis of (—) PAn, (- - -) $[PAn]_{4.8}LiBF_4$, and (— - —)$[PAn]_{2.9}LiBF_4$ films at a frequency of 1 Hz and heating rate of 2 °C/min.

Table 3. Transition Temperatures of PAn, $[PAn]_{4.8}LiBF_4$, and $[PAn]_{2.9}LiBF_4$ Films from Dynamic Mechanical Analysis

		transition temp (°C)			
		α			
sample[a]	PAn/$LiBF_4$ mole ratio[b]	onset	max	end	α′ max
PAn		63	97	144	199
$[PAn]_{4.8}LiBF_4$	4.8	42	109	202	237
$[PAn]_{2.9}LiBF_4$	2.9	97	117	207	>250

[a] All samples contain ~12 weight % NMP (from TGA weight loss at 250 °C). [b] Based on the approximated repeat unit of PAn, $-C_6H_4NH-$.

Table 4. Conductivities of $[PAn]_xLiBF_4$ and $[PAn]_xLiClO_4$ Films Measured at Room Temperature

PAn/salt mole ratio	conductivity (S/cm)	
	$LiBF_4$	$LiClO_4$
9.7/1	1.79×10^{-6}	1.43×10^{-6}
7.3/1	3.73×10^{-6}	3.30×10^{-6}
4.8/1	5.18×10^{-4}	3.03×10^{-4}
2.9/1	2.39×10^{-2}	7.43×10^{-3}

ture.[12] T_α' of the $[PAn]_{4.8}LiBF_4$ is higher than that of PAn (199 °C) by 38 °C.

Conductivity Measurement. The $[PAn]_xLiBF_4$ and $[PAn]_xLiClO_4$ films have conductivities at the same level in the range 10^{-6}–10^{-2} S/cm (Table 4), as determined using the four-point method under dry nitrogen atmosphere. The conductivity increases with increasing content of ionic salt.

During the conductivity measurement of $[PAn]_{2.9}LiBF_4$ and $[PAn]_{2.9}LiClO_4$ films, conductivity fluctuations are only within ~ ± 6% within a time period of 20 min. But for the ionic conducting material, [polyvinyl alcohol]$_6LiBF_4$, the initial conductivity reading (3×10^{-6} S/cm) drops by a factor of 2 after 10 min. This result supports the idea that the ionic salt-doped PAn is an intrinsic conducting material rather than an ionic conducting material. The conductivity of $[PAn]_{2.9}LiBF_4$ film at various temperatures in the range 25–200 °C are shown in Figure 11. It maintains at the level 10^{-2} S/cm in the temperature range 25–140 °C and decays to 10^{-3} S/cm as the temperature increases to 175 °C. The decrease in conductivity can be attributed to the increased ring distortion in the PAn subchains due to the α-relaxation as in the case of neutral poly(3-alkylthiophene) as reported by S.-A.C.[30] It cannot be due to thermal undoping for the reason that there is no generation of quinoid units during the heating scan from 25 to 200 °C as reflected in the absence of the absorption peak at 640 nm[31] (Figure 5). It is unlike the case of HCl doping, in which thermal undoping due to an evaporation of the HCl accompanying a generation of the absorption peak at 640 nm is observed during the heating scan from 25 to 150 °C.

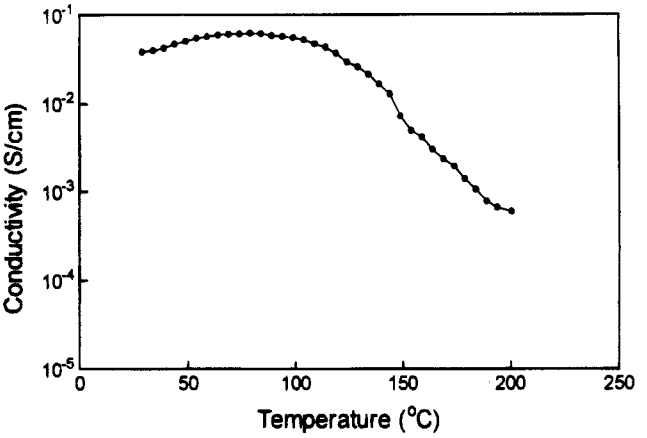

Figure 11. Conductivity versus temperature of $[PAn]_{2.9}LiBF_4$ film from 25 to 200 °C.

Conclusion

Polyaniline (emeraldine base) can be doped by ionic salt via pseudoprotonation of the nitrogens of the imine unit by the metal cations without changing the number of π-electrons in the polymer. A uniformly doped-PAn film can be obtained by casting the NMP solution with PAn and the ionic salt dopant. As in the case of HCl-doped PAn, polarons/bipolarons are also generated. The $LiBF_4$-doped PAn film has a conductivity at the level 10^{-2} S/cm in the temperature range 25–140 °C, which is rather insensitive to the temperature variation in comparison to the HCl-doped PAn. The conductivity then decays to 10^{-3} S/cm as the temperature increases to 175 °C, resulting from the increased ring distortion in the PAn subchains due to the glass transition.

Acknowledgment. We thank the National Science Council of ROC for financial acid through the project NSC 83-0416-E007-01.

References and Notes

(1) Chiang, J. C.; MacDiarmid, A. G. *Synth. Met.* **1986**, *13*, 193.
(2) Genies, E. M.; Lapkowski, M. *Synth. Met.* **1988**, *24*, 61.
(3) Chen, S. A.; Fang, W. G. *Macromolecules* **1991**, *24*, 1242.
(4) Miller, J. S. *Adv. Mater.* **1993**, *5*, 671.
(5) MacDiarmid, A. G.; Chiang, J.-C.; Halpern, M.; Huang, W.-S.; Mu, S.-L.; Somasiri, M. L. D.; Wu, W.; Yaniger, S. I. *Mol. Cryst. Liq. Cryst.* **1985**, *121*, 173.
(6) Travers, J. P.; Chroboczek, J.; Devreux, F.; Genoud, F.; Nechtschein, M.; Syed, A.; Genies, E. M.; Tsintavis, C. *Mol. Cryst. Liq. Cryst.* **1985**, *121*, 195.

(7) MacDiarmid, A. G.; Chiang, J. C.; Richter, A. F.; Epstein, A. J. *Synth. Met.* **1987**, *18*, 285.
(8) Li, S.; Cao, Y.; Xue, Z. *Synth. Met.* **1987**, *20*, 141.
(9) MacDiarmid, A. G.; Epstein, A. J. *Faraday Discuss. Chem. Soc.* **1989**, *88*, 317.
(10) Monkman, A. P.; Adams, P. *Synth. Met.* **1991**, *40*, 87.
(11) Uvdal, K.; Hansan, M. A.; Nillson, J. O.; Salaneck, W. R.; Lungstroem, I.; MacDiarmid, A. G.; Ray, A.; Angelopoulos, A. *Springer Ser. Solid-State Sci.* **1987**, *76*, 262.
(12) Chen, S. A.; Lee, H. T. *Macromolecules* **1993**, *26*, 3254.
(13) Asturias, G. E.; MacDiarmid, A. G.; McCall, R. P.; Epstein, A. J. *Synth. Met.* **1989**, *29*, E157.
(14) Skotheim, T. A. *Handbook of Conducting Polymers*; Marcel Dekker: New York, 1986; Vol. 1, p 224.
(15) Lu, F. L.; Wudl, F.; Nowak, M.; Heeger, A. J. *J. Am. Chem. Soc.* **1986**, *108*, 8311.
(16) Stafstrom, S.; Bredas, J. L.; Epstein, A. J.; Woo, H. S.; Tanner, D. B.; Huang, W. S.; MacDiarmid, A. G. *Phys. Rev. Lett.* **1987**, *59*, 1464.
(17) Furukawa, Y.; Ueda, F.; Hyodo, Y.; Harada, I.; Nakajima, T.; Kawagoe, T. *Macromolecules* **1988**, *21*, 1297.
(18) Chen, S. A.; Lee, H. T. *Synth. Met.* **1992**, *47*, 233.
(19) Salaneck, W. R.; Liedberg, B.; Inganas, O.; Erlandsson, R.; Lundstrom, I.; MacDiarmid, A. G.; Halpern, M.; Somasiri, N. L. D. *Mol. Cryst. Liq. Cryst.* **1985**, *121*, 191.
(20) Tourillon, G. In *Handbook of Conducting Polymers*; Skotheim, T. A., Ed. Marcel Dekker Inc.: New York and Basel, 1986; p 319.
(21) Rieger, P. H. *Electrochemistry*; Prentice-Hall, Inc.: Engelwood Cliffs, NJ, 1987; p 452.
(22) Manohar, S. K.; MacDiarmid, A. G. *Synth. Met.* **1989**, *29*, E349.
(23) Chastain, J., Ed. *Handbook of X-Ray Photoelectron Spectroscopy*; Perkin-Elmer Corp.: Duluth, MN, 1992.
(24) Kang, E. T.; Neoh, K. G.; Khor, S. H.; Tan, K. L.; Tan, B. T. *J. Chem. Soc., Chem. Commun.* **1989**, 695.
(25) Tan, K. L.; Tan, B. T. G.; Kang, E. T.; Neoh, K. G. *Phys. Rev. B* **1989**, *39*, 8070.
(26) Kumar, S. N.; Gaillard, F.; Bouyssoux, G.; Sartre, A. *Synth. Met.* **1990**, *36*, 111.
(27) Inoue, M. B.; Nebesny, K. W.; Fernado, Q.; Inoue, M. *J. Mater. Chem.* **1991**, *1*, 213.
(28) Neoh, K. G.; Kang, E. T.; Tan, K. L. *Polymer* **1993**, *34*, 1630.
(29) Nakajima, T.; Harada, M.; Osawa, R.; Kawagoe, T.; Furukawa, Y.; Hurada, I. *Macromolecule* **1989**, *22*, 2644.
(30) Chen, S.-A.; Ni, J.-M. *Macromolecules* **1992**, *25*, 6081.
(31) Stafstrom, S.; Bredas, J. L.; Epstein, A. J.; Woo, H. S.; Tanner, J. B.; Huang, W. S.; MacDiarmid, A. G. *Phys. Rev. Lett.* **1987**, *59*, 1464.

MA9411540